Optical potential for the n-^{9}Be reaction

Angela Bonaccorso[1] and Robert J. Charity[2]
[1]*INFN, Sezione di Pisa, Largo B. Pontecorvo 3, 56127 Pisa, Italy*
[2]*Department of Chemistry, Washington University, St. Louis, Missouri 63130, USA*
(Received 10 September 2013; revised manuscript received 13 January 2014; published 28 February 2014)

The optical-model potential for the $n + ^9$Be reaction is obtained by two methods. The first method is from a modification and generalization of previous work [Bonaccorso and Bertsch, Phys. Rev. C **63**, 044604 (2001)] and the second is from a dispersive-optical-model fit. The two potentials and also quantities derived from the S matrices used to calculate neutron knockout cross sections are compared.

DOI: 10.1103/PhysRevC.89.024619 PACS number(s): 24.10.Ht, 25.40.Dn

I. INTRODUCTION

This paper is concerned with the search for a phenomenological optical-model potential to reproduce the available experimental data [1] for the total [2], elastic [3–8], and reaction [4,5,7,9–15] cross sections of the system n-^{9}Be. In this paper we refer to all reaction channels different from the elastic channel as "reaction." The original motivation was that ^{9}Be is one of the most commonly used targets in knockout experiments. Theoretical calculations of this process, such as the transfer-to-the-continuum method, need the correct energy dependence of the neutron-target optical potential for the determination of the S matrices [16]. On the other hand, ^{9}Be is in itself a very interesting light nucleus for which various anomalies have been noted in the past, like the large radius and quadrupole moment [17]. Also the seminal Satchler and Love [18] paper on the folding model for ^{9}Be scattering found evidence of anomalously large deformation and surface effects.

We discuss two different methods to obtain the n-^{9}Be phenomenological optical-model potential and we compare their results. One method starts with the use of the potential of Ref. [19] and with its generalization as proposed in Ref. [20]. Here we have extended it to the full range of incident neutron energies for which data are available.

Let us start with Fig. 1, which shows the neutron [2] total cross section in dots (red online), and the available elastic (diamonds, green online) [3–8] and reaction (circles, orange online) cross sections [4,5,7,9,10,12–14]. Because the latter are rather scarce, we have also included proton reaction data (triangles, cyan online) [11–15], which starting from about 20 MeV should represent the effect of the nuclear interaction quite well as the Coulomb effect becomes negligible for these energies. Below about 5 MeV, the total and elastic cross sections are dominated by two resonances which strongly increase the cross section. Conversely at higher energies, the cross section shows a smooth decrease.

On the other hand, one of the most accurate methods for constructing an optical-model potential is the dispersive optical model, DOM, originally introduced in Ref. [21]. It has been traditionally used for stable, heavy nuclei and recently the possibility to extend it to nuclei away from the valley of stability has been explored [22–26]. The DOM was not intended for light nuclei as these have strong deformation effects in the low-energy region, similar to what we have found in n-^{9}Be. However, there have been some attempts to use the DOM for medium mass nuclei, for example, in Refs. [27–29]. In these papers, the n-^{27}Al, n-^{59}Co, n-^{28}Si, n-^{32}S DOM was constructed and some interesting conclusions were drawn, namely that for most deformed nuclei, an analysis of scattering and reaction observables requires that the Schrödinger equation be solved in the coupled-channels framework [30]. It was also found that the Coupled-Channel Method, CCM, is particularly important for achieving a successful description of neutron-nucleus interaction properties at low incident energies E_{inc} <10 MeV, especially for the total cross section and for average resonance parameters [31]. Also a more recent publication [32] applied the DOM to the analysis of neutron and proton scattering on Cr, Fe, and Ni isotopes. In this work a large and comprehensive set of data, including total cross sections, proton reaction cross sections, nucleon elastic and inelastic angular distributions, (p,n) data, and analyzing powers, was analyzed using the dispersive coupled-channels optical model. Furthermore, collective levels and transitions among them were calculated microscopically, finally obtaining an approximate Lane-consistent dispersive coupled-channels optical potential. On the other hand, the importance of introducing deformation effects in order to reproduce the low-energy part of cross sections on light nuclei is also discussed in detail in Refs. [33–35]. In particular those authors pointed out the clear ℓ dependence of the potential, which they attributed to particle-vibration couplings, consistent with what was proposed in Ref. [36].

II. A PHENOMENOLOGICAL N-^{9}BE OPTICAL POTENTIAL

The first method we present here is highly phenomenological as we have constrained our potential (AB) by the simple requirement that the total, elastic, and reaction cross sections from Refs. [1–15] are reproduced. We start with the potential of Ref. [19] obtained from fitting elastic-scattering angular distributions from 9 to 15 MeV and with the extension we made to it in Ref. [20] to cover energies from 20 to 180 MeV. An equally good reproduction of the experimental angular distributions over the 9 to 15 MeV range can be obtained by making the real potential shallower and wider (see Fig. 2). This modification allows for a better reproduction of the lower-energy data, and for even lower energies, a strong surface deformation potential was also introduced to improve

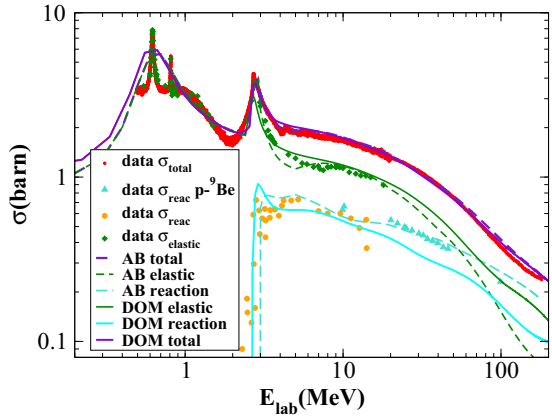

FIG. 1. (Color online) Neutron and proton-^{9}Be experimental and calculated cross sections. Experimental neutron total cross-section data in circles (red online) [2], and the available elastic (diamonds, green online) [3–8] and reaction data [4,5,7,9–15] (proton data, triangles, cyan online; neutron data, circles, orange online). Calculations: total cross section (solid and dashed lines, violet online), elastic cross section (solid and dashed lines, green online), and reaction cross section (solid and dashed lines, cyan online) as indicated in the legend.

the fit to the total cross sections. The final calculated cross sections obtained by an optical-model code are indicated by the dashed curves in Fig. 1.

The AB potential used in the optical-model calculations is defined as follows:

$$U_{AB}(r,E) = -\left[V_{WS}(r,E) + \delta V(r,E) + i\,W_{AB}(r,E)\right]. \quad (1)$$

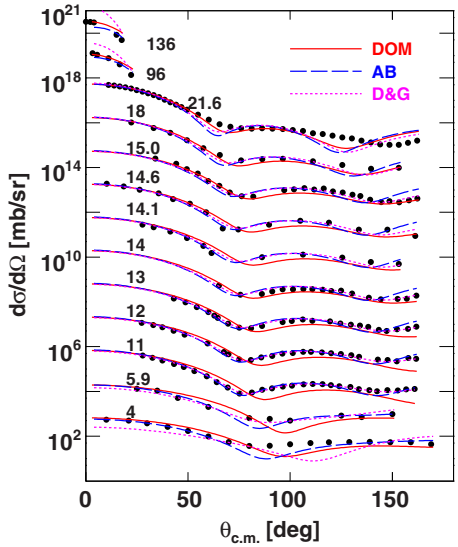

FIG. 2. (Color online) Fitted elastic-scattering angular distributions for $n+{}^9$Be with the dispersive optical model, the AB potential, and the Dave and Gould (DG) potential [19]. The experimental data are from Refs. [6,8,19,37–42]. For display purposes, the fits and data have been successively scaled by a further factor of 30 for each higher neutron energy. Curves and data are labeled by the neutron laboratory energy in MeV.

The real part of the neutron-target interaction is given by V_{WS}, the usual Woods-Saxon potential plus spin-orbit:

$$V_{WS}(r) = V^R f(r,R^R,a^R) - \left(\frac{\hbar}{m_\pi c}\right)^2 \frac{V^{so}}{r}\frac{d}{dr} f(r,R^{so},a^{so})\mathbf{l}\cdot\sigma \quad (2)$$

where the Woods-Saxon form factor is

$$f(r,R^i,a^i) = \frac{1}{1+e^{\frac{r-R^i}{a^i}}} \quad (3)$$

and

$$R^i = r_0^i A^{1/3}. \quad (4)$$

The quantity δV is a correction which originates from surface-deformation effects and represents channels for which a simple Woods-Saxon form is not appropriate. Such couplings suggest the following additional real surface potential [36]:

$$\delta V(r) = 16\alpha e^{2(r-R^R)/a^R} \Big/ \left(1+e^{(r-R^R)/a^R}\right)^4. \quad (5)$$

The imaginary part of the optical-model potential is

$$W_{AB}(r) = W^{\rm vol} f(r,R^I,a^I) - 4a^I W^{\rm sur}\frac{d}{dr} f(r,R^I,a^I). \quad (6)$$

The parameters of $U_{AB}(r,E)$ for the n-^{9}Be interaction used in this paper are given in Table I.

From 0 to 5 MeV, the experimental n-^{9}Be cross section includes some resonances in the elastic scattering that, as expected, the simple phenomenological optical potential cannot reproduce in detail. We have obtained two resonances at $E_{\rm lab} = 0.7$ MeV ($p_{1/2}$) and $E_{\rm lab} = 3.1$ MeV ($d_{5/2}$) using two different parameters for the δV potential of Eq. (5), namely $\alpha = -26.05$ MeV and $\alpha = 3$ MeV. We further discuss such values later. Notice that in the $n+{}^9$Be system, the thresholds for $\alpha+{}^6$He and $2n+{}^8$Be are both below 2 MeV. We have simulated the peak around 2.5 MeV by varying the real potential as the data seem to be dominated by the elastic scattering. Thus the large enhancement of the low-energy cross section is obtained mainly thanks to the surface real term. Starting from 3 MeV, we have a small surface imaginary term which reproduces the reaction data which is probably due to surface oscillations and breakup and also a small volume imaginary potential.

III. A DISPERSIVE OPTICAL MODEL POTENTIAL n-^{9}Be

The second method we present is the dispersive optical model developed by Mahaux and Sartor, of which a complete description can be found in Ref. [21]. The real part of the nucleon self-energy or optical-model potential can be decomposed into an energy-independent nonlocal part and an energy-dependent part, which can also be nonlocal, i.e.,

$$\mathrm{Re}\Sigma(\boldsymbol{r},\boldsymbol{r}';E) = \mathrm{Re}\Sigma(\boldsymbol{r},\boldsymbol{r}';E_F) + \Delta\mathcal{V}(\boldsymbol{r},\boldsymbol{r}';E), \quad (7)$$

where E_F is the Fermi energy and the second term, the dispersive correction, can be determined from the imaginary

TABLE I. Energy-dependent optical-model parameters for the AB potential. $\alpha = -26.05$ MeV for $E_{\rm lab} < 2.4$ MeV, $\alpha = 3$ MeV if $2.4 \leqslant E_{\rm lab} < 10$ MeV, $\alpha = 3.2 - 0.02E_{\rm lab}$ if $E_{\rm lab} \geqslant 10$ MeV; $V^{so} = 7.9$ MeV for $E_{\rm lab} < 2$ MeV, $V^{so} = 5.5$ MeV for $E_{\rm lab} \geqslant 2$ MeV; $r^{so} = 1.27$ fm, $a^{so} = 0.7$ fm; $r_0^I = 1.3$ fm, $a^I = 0.3$ fm at all energies.

$E_{\rm lab}$ (MeV)	V^R (MeV)	r_0^R (fm)	a^R (fm)	$W^{\rm sur}$ (MeV)	$W^{\rm vol}$ (MeV)
$0.1 \leqslant E_{\rm lab} < 3$	$32. - 0.377E_{\rm lab}$	1.647	0.3	0	0
$3 \leqslant E_{\rm lab} < 5$	$31.304 - 0.145E_{\rm lab}$			$0.4 + 1.543(E_{\rm lab} - 3)$	$0.1 + 1.025(E_{\rm lab} - 3)$
$5 \leqslant E_{\rm lab} < 20$		$1.647 - 0.005(E_{\rm lab} - 5)$		$1.65 + 0.365E_{\rm lab}$	$1.0 + 0.23E_{\rm lab}$
$20 \leqslant E_{\rm lab} < 40$			0.3-0.0001$E_{\rm lab}$		$5.6 - 0.005(E_{\rm lab} - 20)$
$40 \leqslant E_{\rm lab} < 111$				$16.25 - 0.05(E_{\rm lab} - 40)$	$5.5 - 0.01(E_{\rm lab} - 40)$
$111 \leqslant E_{\rm lab} < 180$			0.288		4.8

part through the subtracted dispersion relation

$$\Delta\mathcal{V}(\boldsymbol{r},\boldsymbol{r}';E) = +\frac{1}{\pi}\mathcal{P}\int \mathrm{Im}\Sigma(\boldsymbol{r},\boldsymbol{r}';E')\left(\frac{1}{E'-E} - \frac{1}{E'-E_F}\right)dE', \tag{8}$$

where $\mathcal{P}$ stands for the principal value and we note the convention to employ the same sign for the imaginary part of the self-energy above and below the Fermi energy [21]. By definition in Eq. (7) the dispersive correction is zero at the Fermi energy. The dispersive correction varies rapidly around E_F and causes the valence single-particle levels to be focused towards the Fermi energy.

Following Perey and Buck [43], the nonlocal energy-independent term $\mathrm{Re}\Sigma(\boldsymbol{r},\boldsymbol{r}';E_F)$ can be approximated by a local energy-dependent term which Mahaux and Sartor designate as the Hartree-Fock potential $V_{HF}(r,E)$. Strictly this is not a Hartree-Fock potential, but it does describe the effects of the mean field. The energy derivative of V_{HF} is a measure of nonlocality, which is related to the momentum-dependent effective mass

$$\frac{\widetilde{m}(r,E)}{m} = 1 - \frac{dV_{HF}(r,E)}{dE}, \tag{9}$$

where m is the nucleon mass.

A consequence of the local approximation is that one needs to use a scaled imaginary potential

$$W = \frac{\widetilde{m}(r,E)}{m}\mathrm{Im}\,\Sigma \tag{10}$$

and a similarly scaled dispersive correction. The imaginary part of the self-energy is also approximated as a local potential and thus the dispersive correction is correspondingly local. Mahaux and Sartor argue that this modifies $\Delta\mathcal{V}$ by a smooth function of energy which can easily be compensated by a correspondingly smooth modification of V_{HF}. Through these assumptions, the nonlocal self-energy $\Sigma(\boldsymbol{r},\boldsymbol{r}';E)$ can be replaced by an effective energy-dependent local potential

$$U_{\rm DOM}(r,E) = V_{HF}(r,E) + \Delta V(r,E) - iW_{\rm DOM}(r,E). \tag{11}$$

The Fermi energy is defined as

$$E_F = \frac{E_F^+ + E_F^-}{2}, \tag{12}$$

$$E_F^+ = M_{A+1} - (M_A + m), \tag{13}$$

$$E_{sF}^- = M_A - (M_{A-1} + m), \tag{14}$$

where E_F^+ and E_F^- represent the binding energy for adding or removing a nucleon, or alternatively, the single-particle energies of the valence particle and hole states.

A. Parametrization of the DOM potential

Again the imaginary potential is assumed to be composed of the sum of volume and surface components:

$$W_{\rm DOM}(r) = W^{\rm vol}f(r,R^{\rm vol},a^{\rm vol}) - 4a^{\rm sur}W^{\rm sur}\frac{d}{dr}f(r,R^{\rm sur},a^{\rm sur}), \tag{15}$$

but now the radii for the two components are allowed to be different. The phase space of particle levels for $E \gg E_F$ is significantly larger than that of hole levels for $E \ll E_F$. Therefore the contributions from two-particle–one-hole states for $E \gg E_F$ to the self-energy will be larger than that for two-hole–one-particle states at $E \ll E_F$. Thus at energies well removed from E_F, the form of the imaginary volume potential should no longer be symmetric about E_F. Hence the following form was assumed for the depth of the volume potential:

$$W^{\rm vol}(E) = \Delta W_{NM}(E) + \begin{cases} 0 & \text{if } |E - E_F| < E_p^{\rm vol}, \\ A^{\rm vol}\frac{(|E-E_F|-E_p^{\rm vol})^4}{(|E-E_F|-E_p^{\rm vol})^4+(B^{\rm vol})^4} & \text{if } |E - E_F| > E_p^{\rm vol}, \end{cases} \tag{16}$$

where $\Delta W_{NM}(E)$ is the energy-asymmetric correction modeled after nuclear-matter calculations. Apart from this correction, the parametrization is similar to the Jeukenne and Mahaux form [44] used in many DOM analyses.

We set the parameter $E_p^{\rm vol} = 11$ MeV to force the imaginary potential to be zero just in the vicinity of the Fermi energy (see later).

The energy-asymmetric correction was taken as

$$\Delta W_{NM}(E) = \begin{cases} \alpha^{NM} A^{\rm vol}\left[\sqrt{E} + \frac{(E_F+E_a)^{3/2}}{2E} - \frac{3}{2}\sqrt{E_F+E_a}\right] & \text{for } E - E_F > E_a, \\ -A^{\rm vol}\frac{(E_F-E-E_a)^2}{(E_F-E-E_a)^2+(E_a)^2} & \text{for } E - E_F < -E_a, \\ 0 & \text{otherwise,} \end{cases} \quad (17)$$

which is similar to the form suggested by Mahaux and Sartor [21]. Following our previous study [24], we have taken $\alpha^{NM} = 0.08$ MeV$^{-1/2}$ and $E_a = 60$ MeV.

The imaginary surface potential is taken to have the form

$$W^{\rm sur}(E) = \begin{cases} 0 & \text{if } |E - E_F| < E_p^{\rm sur}, \\ \frac{A^{\rm sur}}{1+\exp\left(\frac{|E-E_F|-C^{\rm sur}}{D^{\rm sur}}\right)} \frac{\exp\left(\frac{|E-E_F|-E_p^{\rm sur}}{B^{\rm sur}}\right)-1}{\exp\left(\frac{|E-E_F|-E_p^{\rm sur}}{B^{\rm sur}}\right)+1} & \text{if } |E - E_F| > E_p^{\rm sur}. \end{cases} \quad (18)$$

The Hartree-Fock potential is parametrized in the following way:

$$\begin{aligned} V_{HF}(r,E) = & -V_{HF}^{\rm vol}(E)\ f(r,R^{HF},a^{HF}) \\ & + 4a^{HF} V_{HF}^{\rm sur} \frac{d}{dr} f(r,R^{HF},a^{HF}) \\ & + V^{so}(r,E) + \Delta V(r,E), \end{aligned} \quad (19)$$

where the spin-orbit V^{so} and dispersion ΔV terms have been separated from the volume and surface components.

A real surface term is included in the Hartree-Fock potential. Such a term was required in the DOM analysis of closed-shell nuclei in Ref. [24]. However, in the deformed ^{9}Be system it can also take on the physics contained in the δV term [Eq. (5)] in the AB potential.

The volume component contains the energy-dependence representing nonlocality, which is approximated by the cubic equation

$$\begin{aligned} V_{HF}^{\rm vol}(E) = & V_0^{HF} - \alpha^{\rm vol}(E - E_F) \\ & - \beta^{\rm vol}(E - E_F)^2 - \gamma^{\rm vol}(E - E_F)^3. \end{aligned} \quad (20)$$

The spin-orbit potential was taken to have the standard form, but with an energy-dependent magnitude given by $V_0^{so} - \alpha^{so} E$.

The dispersion correction is related to the imaginary potential through the subtracted-dispersion relationship

$$\Delta V(\boldsymbol{r},E) = +\frac{1}{\pi}\mathcal{P}\int W(\boldsymbol{r},E')\left(\frac{1}{E'-E} - \frac{1}{E'-E_F}\right) dE'. \quad (21)$$

The parameters of the potentials were obtained by simultaneously fitting elastic-scattering angular distributions, reaction, and total cross sections. The fitted angular distributions are displayed in Fig. 2, the calculated total, elastic, and reaction cross sections are the solid curves shown in Fig. 1, while the fitted parameters are listed in Table II. All diffusenesses were fixed to 0.3 fm.

IV. COMPARISON OF THE TWO POTENTIALS

Figure 1 shows that all three cross sections (total, elastic, reaction) obtained with the two potentials are equally good at all energies. The detailed region of the resonances is reproduced naturally by the DOM. On the other hand with the AB potential we need to use two, fixed but not energy-dependent, values for the parameter α in Eq. (5) to achieve the same level of accuracy.

The two real potentials seem to have very similar characteristics. Both potentials contain the effects of the deformation. The DOM has it through the surface term in Eq. (19), the spin-orbit term, and the ΔV term coming from the dispersion relation. The AB has it through the spin orbit and the δV coupling potential, Eq. (5). It seems that the surface term could be interpreted as the results of the combined effect of what in the DOM is the sum of the surface and dispersive terms in

TABLE II. Fixed and fitted parameters from a fit to $n + {}^9$Be data with the dispersive optical model.

E_F	−4.238 MeV
r_0^{HF}	1.287 fm
a^{HF}	0.3 fm
V_0^{HF}	21.87 MeV
$\alpha^{\rm vol}$	0.3259
$\beta^{\rm vol}$	-1.80×10^{-3} MeV^{-1}
$\gamma^{\rm vol}$	3.46×10^{-6} MeV^{-2}
$V_{HF}^{\rm sur}$	12.82 MeV
V_0^{so}	8.768 MeV
α^{so}	0.0261
r_0^{so}	1.230 fm
a^{so}	0.3 fm
$A^{\rm sur}$	12.4 MeV
$B^{\rm sur}$	1.311 MeV
$C^{\rm sur}$	47.08 MeV
$D^{\rm sur}$	39.09 MeV
$E_p^{\rm sur}$	6.60 MeV
$r_0^{\rm sur}$	1.428 fm
$a^{\rm sur} = a^{\rm vol}$	0.3 fm
α^{NM}	0.08 MeV$^{-1/2}$
E_a	60 MeV
$A^{\rm vol}$	3.29 MeV
$B^{\rm vol}$	37.96 MeV
$E_p^{\rm vol}$	11 MeV
$r_0^{\rm vol}$	1.472 fm

Eq. (19). However, this term is more phenomenological than the dispersive term of the DOM.

For the AB potential, we have found that the very low-energy part of the spectrum can be described by a real potential having a conventional Woods-Saxon form plus a surface term. Such term is necessary to reproduce the strong increase of the cross section at low energies. However, the effect of this terms becomes almost negligible at around 20–30 MeV. Deformation effects are common to light nuclei and have been reproduced in various ways. For example, the well-known paper by Comfort and Karp [45] on the $p + {}^{12}$C scattering quotes strong spin-orbit strengths of 6.5 and 7.6 MeV (in our notation) for incident energies of 12 and 22 MeV.

The various parts of the two potentials have been studied and compared in detail for four energy regions. The first is the very-low-energy region where ^{10}Be neutron single-particle levels are important. As the DOM potential was designed to account for both positive- and negative-energy quantities, one might expect it to reproduce this region better. First, the DOM potential reproduced the valence neutron $p_{3/2}$ level by construction as this basically defines the Fermi energy. The $p_{1/2}$ and $d_{5/2}$ levels are calculated to occur at $E_{\text{c.m.}} = 0.58$ and 2.75 MeV, respectively. Note in Fig. 1, these energies correspond to strong enhancements in the total cross sections and the only way to reproduce such structures with the DOM potential is by placing these single-particle resonances at these energies.

If the definition of the phenomenological real potential AB is extrapolated to negative energies it is found that the potential corresponding to the valence neutron separation energy of 6.8 MeV would have $V^R = 34.56$ MeV. We have found that the separation energy of the $p_{3/2}$ valence orbit can be obtained by solving the bound-state Schrödinger equation with $V^R = 31.5$ MeV, if the surface term is put to zero. In this potential we also find the $p_{1/2}$ state, bound by 5.3 MeV, and a narrow ($\Gamma = 0.5$ MeV) $d_{5/2}$ resonance at 3.9 MeV. Using instead the δV surface correction we find a $p_{1/2}$ resonance at $E_{\text{cm}} = 0.606$ MeV ($\Gamma = 0.08$ MeV) while the $d_{5/2}$ resonance occurs at 2.96 MeV ($\Gamma = 0.29$ MeV). Obviously the surface term should be used also in a bound-state calculation, which is automatically achieved by the DOM.

The second comparison has been done at 3 MeV. There one sees that the phenomenological AB potential has a real part that is about 10 MeV deeper than the DOM potential of Sec. II, although the shapes are rather similar. The AB potential has a strong surface term. This is necessary to partially simulate the surface dispersive component, which is present explicitly in the DOM, whose surface term need not to be very strong. The DOM has a surface imaginary part about one order of magnitude larger that the phenomenological AB, and this is at the origin of the important dispersive component in the real part. This component allows for the smooth and continuous increase of the total and elastic cross sections below 20 MeV.

We have then looked at the intermediate-energy region, taking as an example $E_{\text{inc}} = 20$ MeV. In this case the two potentials have very similar surface terms, with a depth of about 8 MeV, but while the DOM has a small volume imaginary part, the AB potential has a Woods-Saxon volume with a depth

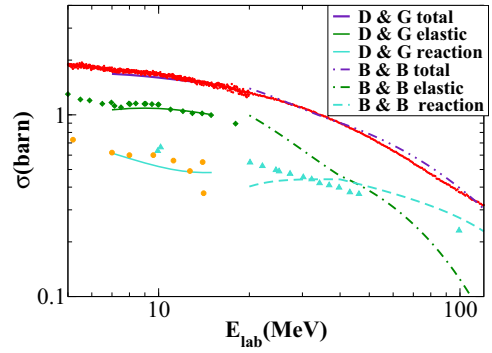

FIG. 3. (Color online) Cross sections calculated with the potentials of Dave and Gould (DG) [19] and Bonaccorso and Bertsch (BB) [20]. The data are the same as in Fig. 1.

of about 6 MeV, thus giving a bit more absorption in total. Finally in the high-energy region at $E_{\text{inc}} = 80$ MeV, the AB volume potential has decreased very slightly while the surface potential has become about 30% deeper. The DOM potential has for both terms a depth of about 3 MeV. Thus its volume part is quite close to the corresponding AB part, while the surface is about five times smaller. In this region the AB cross sections are dominated by the reaction component while the DOM gives similar amounts of elastic and reaction cross section.

Figure 3 shows the same data as Fig. 1 and the cross sections calculated according to Refs. [19,20] in the energy range for which each potential was fitted, namely 9–15 MeV for Ref. [19] and 20–180 MeV for Ref. [20]. Notice that both the DOM and the AB potentials provide more accurate reproductions of the elastic and reaction data as indicated by Fig. 1. Furthermore they extend over a much larger energy range including very low energies.

Figure 2 displays the elastic-scattering angular distributions calculated according to the DOM and AB potentials and also with the potential of Ref. [19]. They are compared to the available data from Refs. [6,8,19,37–42]. All calculations give reasonable fits to the experimental data except for the potential from Ref. [19] at the highest two energies ($E_{\text{lab}} = 96$ and 136 MeV). The latter is not surprising as the potential from

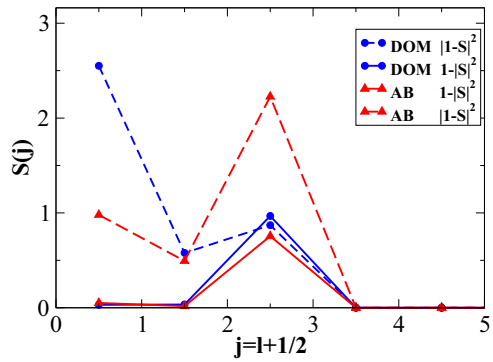

FIG. 4. (Color online) The quantities $|1 - S|^2$ and $1 - |S|^2$ calculated with the two optical-model potentials for a neutron bombarding energy of 3 MeV.

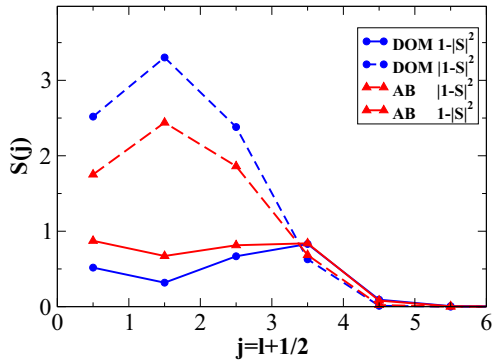

FIG. 5. (Color online) Same as for Fig. 4, but for a neutron bombarding energy of 20 MeV.

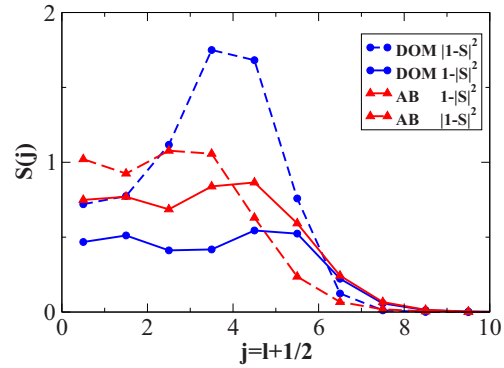

FIG. 6. (Color online) Same as for Fig. 4, but for a neutron bombarding energy of 80 MeV.

Ref. [19] was fit just in the 9–15 MeV region. Overall the AB potential reproduces the data somewhat better than the DOM potential, but we note that experimental angular distributions covering the full angular range are available only for a small range of neutron energies.

V. *S* MATRIX

In neutron knockout calculations, the neutron-target S matrix is needed in both the transfer-to-the-continuum method [16] and the eikonal method [46]. In both methods, the knockout cross section is separated into two components: an elastic or diffraction component where the knocked-out neutron interacts elastically with the target and an inelastic or stripping component where the neutron elastic flux is absorbed. The quantities $|1 - S|^2$ and $1 - |S|^2$ are used to calculate these components, respectively.

These quantities, calculated from the two potentials at 3, 20, and 80 MeV, are plotted in Figs. 4 to 6 as a function of the total angular momentum $j = l + 1/2$. By using the semiclassical relation $l + 1/2 = bk$ where b is the n-target impact parameter and k is the momentum of relative motion, one can deduce from these figures an impact-parameter dependence for the S matrix. Similar plots could be made for the case $j = l - 1/2$.

The quantity $1 - |S|^2$ is of course bounded by unity, which would represents complete absorption of the elastic flux by the target. Even at small j values, we see some transparency with both potentials for the two higher energies (20 and 80 MeV). In these figures, the calculations with the two potentials show some significant differences. The most important angular momenta for knockout reactions are the more peripheral collisions, where the quantity $1 - |S|^2$ is more similar for the two potentials at all energies. The quantity $|1 - S|^2$ calculated with the DOM consistently gives a larger contribution for larger j values at 20 and 80 MeV. Calculations with the two potentials can be used to gauge the uncertainty in the neutron-target S matrix to the predicted cross sections.

VI. CONCLUSION

In this paper, we have presented and compared two parametrizations of the optical-model potential for the system n-^{9}Be over a large energy range. To our knowledge, this is the first time that such an effort is presented in the literature for a very light system and with two independent methods. The two potentials have similar features. Namely, both present unusually strong real surface terms in the low-energy region, which are necessary to reproduce the steep enhancement of the cross section. We interpret this effect as representative of strong surface deformation and related channel couplings. This is the most interesting aspect of the present work which allows for a microscopic interpretation of the potentials. An important surface term for both potentials is also necessary in the imaginary part. Volume terms are present in both potentials, but with lesser strength, in agreement with the common understanding of light nuclei dynamics as dominated by surface properties. While the DOM potential provides naturally an excellent reproduction of the cross sections at all energies including the resonance region, the simple optical-model potential does not contain the necessary ingredients to reproduce the details of the resonant parts of the excitation function and needs a surface phenomenological correction to achieve comparable results. This is interpreted as a need for the dispersive term contained in the DOM. We believe that such findings could have a strong impact in the studies of light exotic nuclei, in particular neutron-unbound nuclei, for which it is very important to obtain a unified description of states around the particle-emission threshold.

ACKNOWLEDGMENTS

The work of one of us (R.J.C.) was supported by the U.S. Department of Energy, Division of Nuclear Physics, under Grant No. DE-FG02-87ER-40316. A.B. acknowledges many enlightening discussions with the late Nicole Vinh Mau.

[1] EXFOR nuclear data library [http://www-nds.iaea.org/exfor/exfor.htm].
[2] R. W. Finlay *et al.*, Phys. Rev. C **47**, 237 (1993).
[3] H. H. Hogue, P. L. Von Behren, D. H. Epperson, S. G. Glendinning, P. W. Lisowski, C. E. Nelson, H. W. Newson, F. O. Purser, W. Tornow, C. R. Gould, and L. W. Seagondollar, Nucl.

Sci. Eng. **68**, 38 (1978); D. M. Drake, G. F. Auchampaugh, E. D. Arthur, C. E. Ragan, and P. G. Young, *ibid.* **63**, 401 (1977); J. P. Chien and A. B. Smith, *ibid.* **26**, 500 (1966); D. D. Phillips, Washington AEC Office Report No. 1028, 29, 1960 (unpublished); H. B. Willard, J. K. Bair, and J. D. Kington, Phys. Rev. **98**, 669 (1955); A. Langsdorf Jr., R. O. Lane, and J. E. Monahan, *ibid.* **107**, 1077 (1957); M. P. Nakada, J. D. Anderson, C. C. Gardner, and C. Wong, *ibid.* **110**, 1439 (1958); R. O. Lane, A. J. Elwyn, and A. Langsdorf Jr., *ibid.* **133**, B409 (1964); R. O. Lane and J. E. Monahan, Argonne National Laboratory Report No. 5554, 22, 1956 (unpublished); J. A. Templon, J. H. Dave, C. R. Gould, and S. Singkarat, Nucl. Sci. Eng. **91**, 451 (1985) ; M. Sugimoto, P. T. Guenther, J. E. Lynn, A. B. Smith, and J. F. Whalen, *ibid.* **103**, 37 (1987); H. H. Barschall, M. E. Battat, W. C. Bright, E. R. Graves, T. Jorgensen, and J. H. Manley, Phys. Rev. **72**, 881 (1947); M. Baba, T. Sakase, T. Nishitani, T. Yamada, and T. Momota, in *Proceeding of the International Conference on Neutron Physics and Nuclear Data for Reactors and other applied purposes* (OECD publications, Harwell, 1978); F. Merchez, V. Regis, N. Van Sen, R. Darves-Blanc, P. Dinh Lien, and R. Bouchez, in *Nuclear Data for Reactors Conference* (IAEA, Paris, 1966); Report from Euratom Countries, EANDC Report No. 89U, 234, 1968 (unpublished); A. Takahashi, E. Ichimura, Y. Sasaki, and H. Sugimoto, Osaka University OKTAVIAN Report No. 87, 03, 1987 (unpublished); D. Schmidt, W. Mannhart, and S. Khurana, Phys. Techn. Bundesanst. Neutronenphysik Report No. 55, 2007 (unpublished); C. Guanren, W. Shenlin, H. Tangzi, B. Xixiang, and Li Anli, Chin. J. Nucl. Phys. (Beijing) **3**, 320 (1981); S. Guanren, W. Shenlin, H. Tangzi, L. Anli, and Bai Xixiang, Nucl. Sci. Eng. **86**, 184 (1984); G. V. Gorlov, N. S. Lebedeva, and V. M. Morozov, Doklady Akademii Nauk. **158**, 574 (1964); D. I. Lyapin, L. V. Mitsyna, A. B. Popov, I. M. Salamatin, and G. S. Samosvat, Joint Inst. for Nucl. Res. Dubna Report No. 89, 408, 1989 (unpublished).

[4] M. Walt, J. R. Beyster, Phys. Rev. **98**, 677 (1955).

[5] J. B. Marion, J. S. Levin, and L. Cranberg, Phys. Rev. **114**, 1584 (1959).

[6] N. Olsson, E. Ramstrom, and B. Trostell, Nucl. Phys. A **509**, 161 (1990).

[7] J. S. Levin and L. Cranberg, Washington AEC Office Report No. 1029, 44, 1960 (unpublished).

[8] J. Chen, P. Zhu, X. Mao, X. Li, G. Shen, J. Zhang, and Y. Han, Ann. Nucl. Energy **36**, 668 (2009).

[9] D. Didier and H. Dilleman, J. Phys (Paris) **24**, 805 (1963).

[10] J. R. Beyster, R. L. Henkel, R. A. Nobles, and J. M. Kister, Phys. Rev. **98**, 1216 (1955); H. L. Taylor, O. Lonsjo, and T. W. Bonner, *ibid.* **100**, 174 (1955); J. R. Beyster, M. Walt, and E. W. Salmi, *ibid.* **104**, 1319 (1956); M. H. Mac Gregor, W. P. Ball, and R. Booth, *ibid.* **108**, 726 (1957); **111**, 1155 (1958); W. P. Ball, M. MacGregor, and R. Booth, *ibid.* **110**, 1392 (1958); D. R. Weaver and J. Walker, J. Phys. D **7**, 1122 (1974); J. R. P. Eaton and J. Walker, in *Proceedings of Nuclear Cross Sections and Technology Conference* (Washington, 1968). NBS special publication 299; A. V. Cohen, J. Nucl. Energy, Parts A/B **14**, 180 (1961); Report from Euratom-countries and Euratom to EANDC, Report No. 49, 85, 1963 (unpublished); M. H. Mc Taggart, and H. Goodfellow, J. Nucl. Energy, Parts A/B **17**, 437 (1963); N. N. Flerov and V. M. Talysin, Atom. Ener. **1**, 155 (1956); V. M. Gorbachev and L. B. Poretskij, *ibid.* **4**, 191 (1958).

[11] I. Slaus, D. J. Margaziotis, R. F. Carlson, W. T. H. van Oers, and J. R. Richardson, Phys. Rev. C **12**, 1093 (1975).

[12] D. G. Montague, R. K. Cole, M. Makino, and C. N. Waddell, Nucl. Phys. A **199**, 457 (1973).

[13] W. F. McGill, R. F. Carlson, T. H. Short, J. M. Cameron, J. R. Richardson, I. Slaus, W. T. H.van Oers, J. W. Verba, D. J. Margaziotis, and P. Doherty, Phys. Rev. C **10**, 2237 (1974).

[14] B. D. Wilkins and G. Igo, Phys. Rev. **129**, 2198 (1963).

[15] P. Kirkby and W. T. Link, Can. J. Phys. **44**, 1847 (1966); A. Ingemarsson, J. Nyberg, P. U. Renberg, O. Sundberg, R. F. Carlson, A. Auce, R. Johansson, G. Tibell, B. C. Clark, L. Kurth Kerr, and S. Hama, Nucl. Phys. A **653**, 341 (1999).

[16] A. Bonaccorso, Phys. Rev. C **60**, 054604 (1999); A. Bonaccorso and F. Carstoiu, *ibid.* **61**, 034605 (2000).

[17] D. R. Tilley, J. H. Kelley, J. L. Godwin, D. J. Millener, J. Purcell, C. G. Sheu, and H. R. Weller, Nucl. Phys. A **745**, 155 (2004).

[18] G. R. Satchler and W. G. Love, Phys. Rep. **55**, 183 (1979).

[19] J. H. Dave and C. R. Gould, Phys. Rev. C **28**, 2212 (1983).

[20] A. Bonaccorso and G. F. Bertsch, Phys. Rev. C **63**, 044604 (2001).

[21] C. Mahaux and R. Sartor, Adv. Nucl. Phys. **20**, 1 (1991).

[22] R. J. Charity, L. G. Sobotka, and W. H. Dickhoff, Phys. Rev. Lett. **97**, 162503 (2006).

[23] R. J. Charity, J. M. Mueller, L. G. Sobotka, and W. H. Dickhoff, Phys. Rev. C **76**, 044314 (2007).

[24] J. M. Mueller, R. J. Charity, R. Shane, L. G. Sobotka, S. J. Waldecker, W. H. Dickhoff, A. S. Crowell, J. H. Esterline, B. Fallin, C. R. Howell, C. Westerfeldt, M. Youngs, B. J. Crowe, III, and R. S. Pedroni, Phys. Rev. C **83**, 064605 (2011).

[25] W. H. Dickhoff and C. Barbieri, Prog. Part. Nucl. Phys. **52**, 377 (2004).

[26] C. Barbieri, Phys. Rev. Lett. **103**, 202502 (2009).

[27] M. M. Nagadi, C. R. Howell, W. Tornow, G. J. Weisel, M. A. Al-Ohali, R. T. Braun, H. R. Setze, Z. Chen, R. L. Walter, J. P. Delaroche, and P. Romain, Phys. Rev. C **68**, 044610 (2003).

[28] M. M. Nagadi, Ph.D. dissertation, Duke University, 1992 (unpublished); (private communication).

[29] M. A. Al-Ohali, J. P. Delaroche, C. R. Howell, M. M. Nagadi, A. A. Naqvi, W. Tornow, R. L. Walter, and G. J. Weisel, Phys. Rev. C **86**, 034603 (2012).

[30] T. Tamura, Rev. Mod. Phys. **37**, 679 (1965).

[31] J. P. Delaroche, Ch. Lagrange, and J. Salvy, *Nuclear Theory in Neutron Nuclear Data Evaluation* (IAEA, Vienna, 1976), Vol. II, p. 251.

[32] R. Li, Weili Sun, E. Sh. Soukhovitskii, J. M. Quesada, and R. Capote, Phys. Rev. C **87**, 054611 (2013), and references therein.

[33] R. R. Winters, C. H. Johnson, and A. D. MacKellar, Phys. Rev C **31**, 384 (1985).

[34] G. H. Rawitscher and D. Lukaszek, Phys. Rev. C **69**, 044608 (2004).

[35] A. D. MacKellar and B. Castel, Phys. Rev. C **29**, 1993 (1984); **28**, 441 (1983).

[36] N. Vinh Mau and J. C. Pacheco, Nucl. Phys. A **607**, 163 (1996).

[37] C. P. Van Zyl, R. G. P. Voss, and R. Wilson, Philos. Mag. **1**, 1003 (1956).

[38] G. L. Salmon, Nucl. Phys. **21**, 15 (1960).

[39] G. V. Gorlov, Dok. Akad. Nauk SSSR **158**, 574 (1964).

[40] L. F. Hansen, F. S. Dietrich, B. A. Pohl, C. H. Poppe, and C. Wong, Phys. Rev. C **31**, 111 (1985).
[41] N. Baba, M. Ishikawa, T. Kikuchi, H. Wakabayashi, N. Yabuta, and N. Hirakawa, in *Nuclear Data for Science and Technology: Proceedings of the International Conference, 1988, Mito, Japan* (Saikon Publishing, Tokyo, 1988).
[42] M. Ibaraki, M. Baba, S. Matsuyama, T. Sanami, T. Win, T. Miura, and N. Hirakawa, J. Nucl. Sci. Technol. **35**, 843 (1998).
[43] F. Perey and B. Buck, Nucl. Phys. **32**, 252 (1962).
[44] J. P. Jeukenne and C. Mahaux, Nucl Phys. **A394**, 445 (1983).
[45] J. R. Comfort and B. C. Karp, Phys. Rev. C **21**, 2162 (1980).
[46] P. G. Hansen and J. A. Tostevin, Ann. Rev. Nucl. Part. Sci. **53**, 219 (2003).